Turbulent Vertical Kinetic Energy in the Ocean Mixed Layer

ERIC A. D'ASARO

Applied Physics Laboratory and School of Oceanography, University of Washington, Seattle, Washington

(Manuscript received 9 November 2000, in final form 21 May 2001)

ABSTRACT

Vertical velocities in the ocean boundary layer were measured for two weeks at an open ocean, wintertime site using neutrally buoyant floats. Simultaneous measurements of the surface meteorology and surface waves showed a large variability in both wind and wave properties and only weak correlations between them. Buoyancy forcing was weak. The mean square vertical velocity in the boundary layer σ_w^2 measured from the vertical motion of the floats was proportional to the squared friction velocity u_*^2 estimated from shipboard meteorological measurements using bulk formulas. Thus $\sigma_w^2 = \overline{A}u_*^2$ (the rate of momentum transport from the atmosphere to the ocean is ρu_*^2, where ρ is the density of the water). The deviations from this relation can be attributed entirely to statistical variation and measurement error. The measured values of σ_w^2 were corrected for measurement biases and the nonturbulent contributions of internal waves. The value of the turbulent part of $\overline{A}$ is 1.75–2 times that measured in laboratory and oceanic solid-wall turbulent boundary layers driven by shear alone. Although surface waves undoubtedly play a large role in the physics of the oceanic boundary layer, their effects on vertical velocity variance are remarkably well parameterized by wind stress in this data.

1. Introduction

Measurements of turbulence properties in the ocean boundary layer are limited. Accordingly, present models of the ocean boundary layer are constructed primarily by analogy with atmospheric boundary layers over land. Over land, the fluid velocity must be zero at the surface but is finite at altitude. Turbulence is generated by instabilities of this sheared flow and carries a vertical flux of horizontal momentum, a stress. In the oceanic analog, the wind stress τ acts to accelerate the ocean surface downwind, thereby setting up an unstable sheared flow in the upper ocean. Instabilities in this flow produce turbulent velocity fluctuations whose average amplitude is proportional to the friction velocity $u_* = \sqrt{\tau/\rho}$, and thus depend on the stress τ. If this is the only source of turbulence, the vertical velocity variance σ_w^2 at depth z is given by

$$\sigma_w^2 = A\,(z)u_*^2, \tag{1}$$

and the vertical velocity variance in the mixed layer is given by

$$\overline{\sigma_w^2} = \overline{A}u_*^2, \tag{2}$$

where the overbar denotes the vertical averaging operation.

Corresponding author address: Eric A. D'Asaro, Applied Physics Laboratory, University of Washington, 1013 NE 40th St., Seattle, WA 98105.
E-mail: dasaro@apl.washington.edu

Surface gravity waves make the ocean surface different from the land surface. Gravity waves contain most of the energy in the boundary layer and thus play a large role in the physics of the boundary layer turbulence (Melville 1994). The waves may break, thereby transferring some of their energy and momentum to turbulence and injecting clouds of buoyant bubbles into the ocean. Waves may also be refracted by the nonwave velocities, thereby transferring momentum from the waves to the turbulence. This process, the Craik–Leibovich (CL: Leibovich 1983) interaction, is thought to generate downwind-aligned, counterrotating vortices known as Langmuir cells. The Stokes drift (Phillips 1977) is often used as the key wave parameter in this interaction. Finally, the periodic straining of the turbulence by the surface waves may increase turbulent dissipation (Thais and Magnaudet 1996). It therefore seems sensible that the properties of the oceanic boundary layer should be sensitive to the properties of the surface gravity wave field and thus exhibit a more complex dependence than hypothesized by (1) and (2). We test this sensitivity here.

2. Measurements

Turbulent velocity fluctuations in the oceanic boundary layer are typically a few centimeters per second, much smaller than the one meter per second typical velocities of surface waves. This presents a formidable measurement challenge. This can be overcome by measuring the motion of neutrally buoyant ''Lagrangian

floats'' (D'Asaro et al. 1996). These are designed to follow the three-dimensional motion of water parcels within the boundary layer by maintaining a neutral buoyancy and by having a large drag. The depth of the float is measured using an onboard pressure sensor; its vertical velocity is measured from the rate of change of pressure.

There are two major sources of error in the float's measurement of vertical velocity. First, the floats are slightly buoyant (about 0.5–3 g), a feature imposed to ensure that they do not sink out of the mixed layer. A circular metal drogue with a frontal area of about 1 m^2, acted upon by this buoyancy, results in an upward motion of 3–5 mm s^{-1} of the floats relative to the water. The floats therefore are not exactly Lagrangian and do not necessarily sample the mixed layer uniformly. The magnitude of the resulting error is discussed later in this paper. Second, the approximately 1-m size of the float reduces its response to velocity fluctuations smaller than itself (Lien et al. 1998). This has only a minor effect on the measured velocity variance since most of the velocity variance is at scales larger than the float size.

Surface waves are not an important source of noise in these measurements for several reasons. Pressure fluctuations are zero along particle paths for linear surface waves, thus greatly attenuating the surface wave pressure fluctations measured by the float. The float pressure sensor is mounted at the top of the float and therefore does not exactly follow a particle path. D'Asaro et al. (1996), using float and surface wave measurements, show that the float pressure signal at surface wave frequencies is explained by a model in which the center of the float follows a Lagrangian path and the waves are linear. The pressure fluctuations measured at the float are much less than the surface wave pressure fluctuations in the same depth range. Surface waves are not exactly linear. However, the lowest-order contribution of surface wave nonlinearity to the surface pressure is due to the wave dynamic pressure $\rho U^2/2$ where U is the wave velocity (Phillips 1977). For $U = 1$ m s^{-1}, this is equivalent to only $\delta_{NL} = 0.05$ m of depth variation. The wave amplitude δ_{NL} will vary with a period of roughly 100 seconds as wave groups propogate past the float. This contributes only about 0.003 m s^{-1} to the measured float velocity, which is negligible. The small remaining velocity fluctuations at surface wave frequencies are sampled at 1 Hz and reduced to a negligible level by using a 50-s running mean sampled at a 25-s period. Lien et al. (1998) and D'Asaro and Lien (2000) show that Lagrangian frequency spectra of vertical velocity have the same spectral shape in turbulent flows with and without surface waves.[1] The vertical velocity variance is concentrated at frequencies far lower than those of surface waves. If surface waves contributed significantly to the velocity spectra, one would expect spectra taken from environments with surface waves to differ from those taken in wave-free environments. None of this is meant to imply that surface waves are unimportant in the dynamics of the mixed layer, only that they do not affect the measurement of float depth from pressure.

Three Lagrangian floats were deployed from the Research Vessel *Wecoma* for two weeks in deep water off the coast of Vancouver Island in January 1995. The experiment followed the drifting floats 70 km northward from 48.0°N, 127.9°W in 2400–2500 m of water. Their depth–time trajectories are shown in Fig. 1b. Each float was deployed for approximately 24 hours, recovered, and redeployed with its density adjusted to compensate for the slowly changing density of the mixed layer. Frequent vertical profiles of temperature and salinity were made using a SeaBird 9/11 CTD with redundant sensors.[2] The CTD profiles were used to define the depth of the mixed layer[3] shown by the heavy orange line in Fig. 1b. Individual floats (Fig. 2) moved vertically between the sea surface and approximately the mixed layer depth. Floats placed below the mixed layer (not shown here) are constrained vertically by the strong stratification and undergo much smaller vertical excursions. This illustrates the rapid vertical exchange characteristic of the turbulent boundary layer.

Fluxes of buoyancy and momentum were computed from the meteorological measurements on the *Wecoma* using bulk formulas and are shown in Fig. 1a. Downwelling shortwave and longwave radiation were measured with redundant Eppley radiometers adjusted following Dickey et al. (1994). Temperature, humidity, and wind speed and direction were measured using redundant sensors. Temperature data were screened for occasional coolings due to spray. Wind data from the upwind side of the ship were used. Fluxes were calculated following Fairall et al. (1996) as implemented in the MATLAB Air–Sea toolbox version 2.0 (http://sea-mat.whoi.edu/). Buoyancy flux is the sum of that due to shortwave and longwave radiation and that due to sensible and latent heat fluxes. Average values of these quantities are 41, −22, 4, and −27 W m^{-2}, respectively.

[1] Although Lien et al. (1998) include data from the measurements described in this paper, they include only data from depths deeper than 15 m. Spectra from depths shallower than 15 m have very similar shapes as long as only data from mixed layers deeper than 20 m and u_* greater than 0.008 m s^{-1} are considered.

[2] Occasional bottle samples were taken and used to verify that the measured salinity was correct to 0.005 psu. Short-term precision of temperature and salinity is better than 0.001°C and 0.001 psu, respectively.

[3] The mixed layer depth was defined as the shallowest depth at which the density deviation from the shallowest good value was greater than 0.003 kg m^3. The mixed layer depths computed from individual profiles were linearly interpolated onto a fine grid and subjected to a 3.8-h running mean (very close to the averaging time for σ_w). Note that this mixed layer depth is shallower than the top of the main thermocline H_{mt} as defined by a deviation of 0.1 kg m^3 from the surface density. The value of H_{mt} slowly increased from about 72 m to about 80 m during the 2 weeks of measurement.

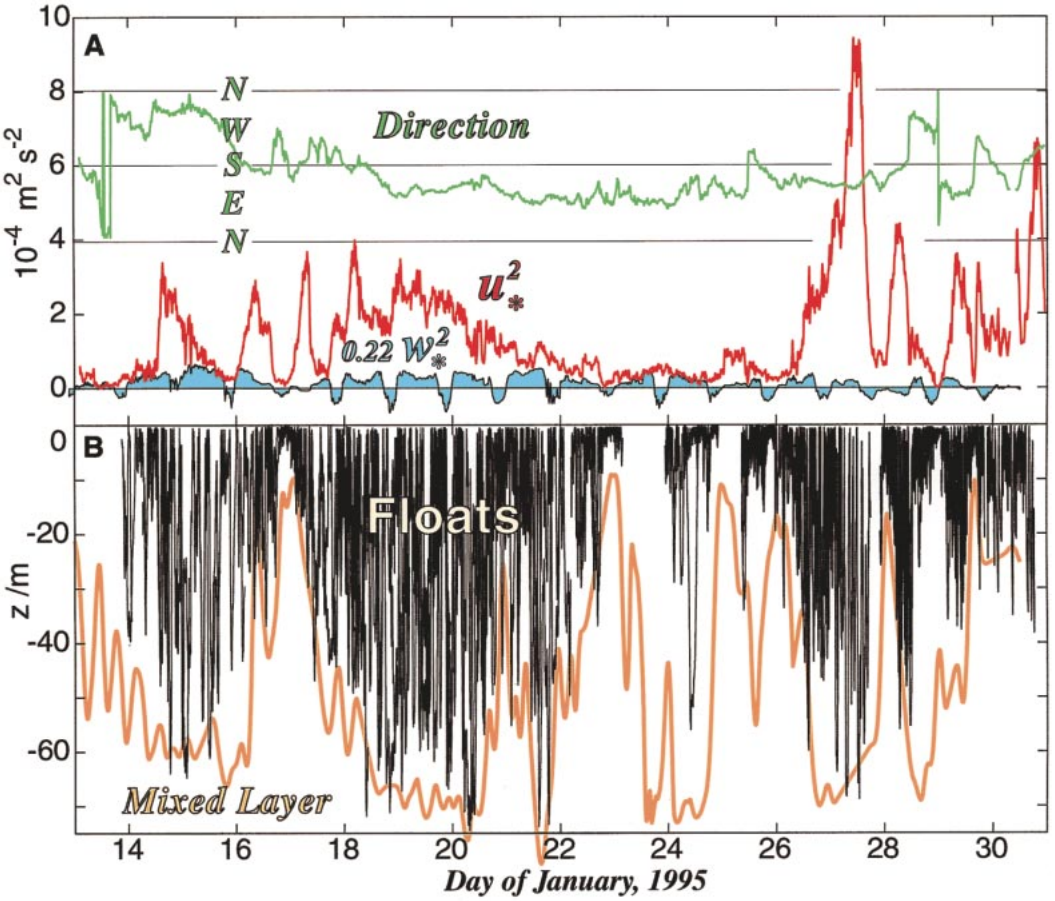

FIG. 1. (a) Meteorological forcing. Wind stress τ (red) is represented by $u_*^2 = \tau/\rho$ and buoyancy flux J_b (blue) is represented by $w_*^2 = (J_b H)^{2/3}$; w_*^2 is scaled relative to u_*^2 in approximate proportion to their ability to force vertical motions in the mixed layer. (The mean square vertical velocity in free convection is about $0.3w_*^2$ (Stull 1988); here the mean square vertical velocity forced by wind stress is $1.35u_*^2$; (a) therefore scales w_*^2 by $0.22 = 0.3/1.35$.) Positive values of w_*^2 imply cooling of the ocean; negative values of w_*^2 imply heating. Direction from which the wind is blowing is shown in green. (b) Depth–time trajectories of floats during experiment. Mixed layer depth H is shown in orange.

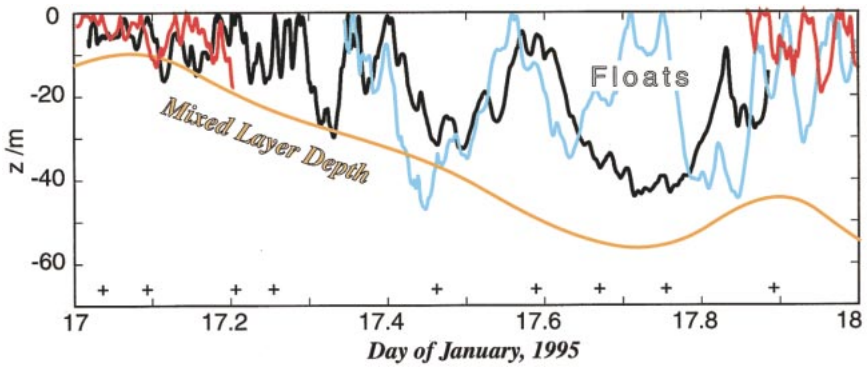

FIG. 2. Depth–time trajectories of floats during one typical day of data. Portions of four float deployments occur during this day as indicated by the red, black, and blue lines. The mixed layer depth, computed from density profiles, is shown in orange. Times of individual density profiles are shown by pulses.

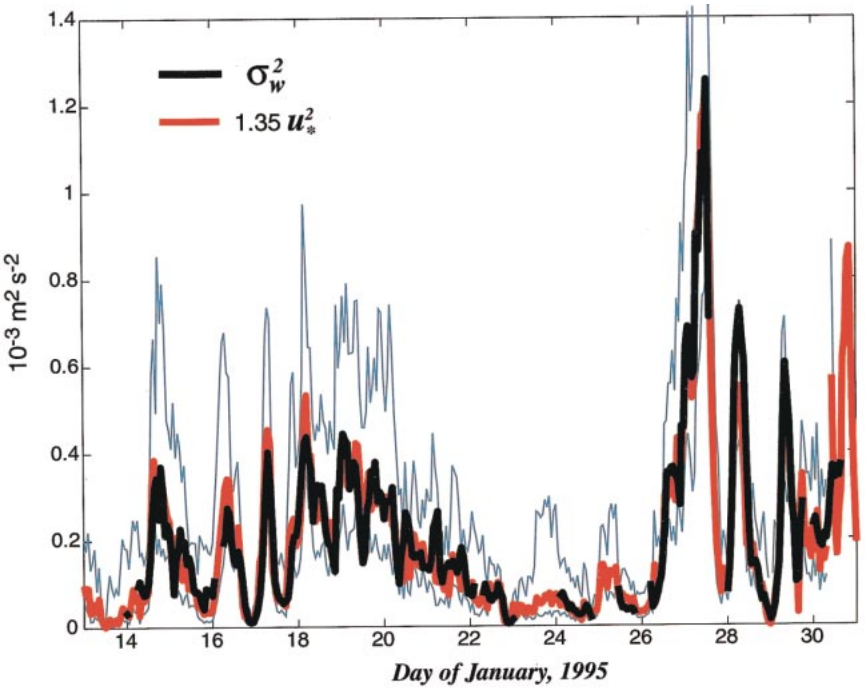

FIG. 3. Mean square vertical velocity σ_w^2 and squared friction velocity u_*^2. Gray lines are 95% confidence limits of a χ^2 distribution. (Degrees of freedom for each average over $T_{av} = 3.6$ h and n_{floats} floats is $(T_{av}/T_c)(\langle 1/\tau\rangle/\tau)n_{floats}$, where $\tau = H/u_*$ is proportional to the time needed for a float to cross the mixed layer and $\langle 1/\tau\rangle$ is the time average of $1/\tau$. The correlation time $T_c = 750$ s was estimated from the overall ratio of the mean to the standard deviation assuming a χ^2 distribution.)

Large variations in wind stress occurred as a series of small storms swept past the site. The depth of the mixed layer tended to increase during periods of strong wind, as expected, since increased wind leads to increased vertical mixing. The depth of the mixed layer tended to decrease during periods of weak wind. This is probably due to the relaxation of horizontal density gradients into the vertical (Rudnick and Ferrari 1999).

3. Analysis and results

The vertical velocity variance σ_w^2 was estimated from the 3.6-h average of all float vertical velocities. Since each float traverses the mixed layer several times during the averaging period, σ_w^2 corresponds approximately to the mixed layer average of w^2. Comparison of the time series of u_*^2 and σ_w^2 (Fig. 3) shows a close correspondence. Further averaging of σ_w^2 to reduce the sampling error shows that almost all the variation in σ_w^2 is due to u_*^2 (Fig. 4). Equation (2) is remarkably accurate for these data.

Although buoyancy flux is often the major source of boundary layer turbulence in the oceanic boundary layer at other times and places (Lien et al. 1998; Steffen and D'Asaro 2001) it is of minor significance in these data. No relationships were found between the buoyancy forcing and σ_w^2. Time series of w_*^2 are uncorrelated with u_*^2, σ_w^2 and that part of σ_w^2 that is uncorrelated with u_*^2.

No relationships were found between surface wave properties and σ_w^2 except those that could be explained by correlations between wave properties and u_*. Scalar surface wave spectra were measured using a single-beam upward-looking sonar mounted on a stable subsurface platform; directional surface wave spectra were measured from a horizontally scanning sonar mounted on a similar platform (Trevorrow 1995). The directional spectra often exhibited complex multipeaked forms reflecting the rapidly changing and spatially variable storm structure. Measured spectra were used to compute various surface wave properties. Figure 5 shows the time series of measured wave height squared σ_ζ^2 and a prediction of σ_ζ^2 dependent only on the local wind and wind stress.[4] The measured wave height increases when the wind increases but can remain high for several days after the wind decreases. The wave energy per unit area E_{wave} and the wave phase speed at the peak of the wave displacement spectrum C_{peak} are only weakly correlated with u_*. The wave slope at the peak of the spectrum

[4] The model spectrum for the scalar surface wave spectrum is the Phillips (1985) spectrum, which depends only on u_*, modified by the Pierson and Moskowitz (1964) peak function, which depends only on U_{20}, the wind speed at 20 m height.

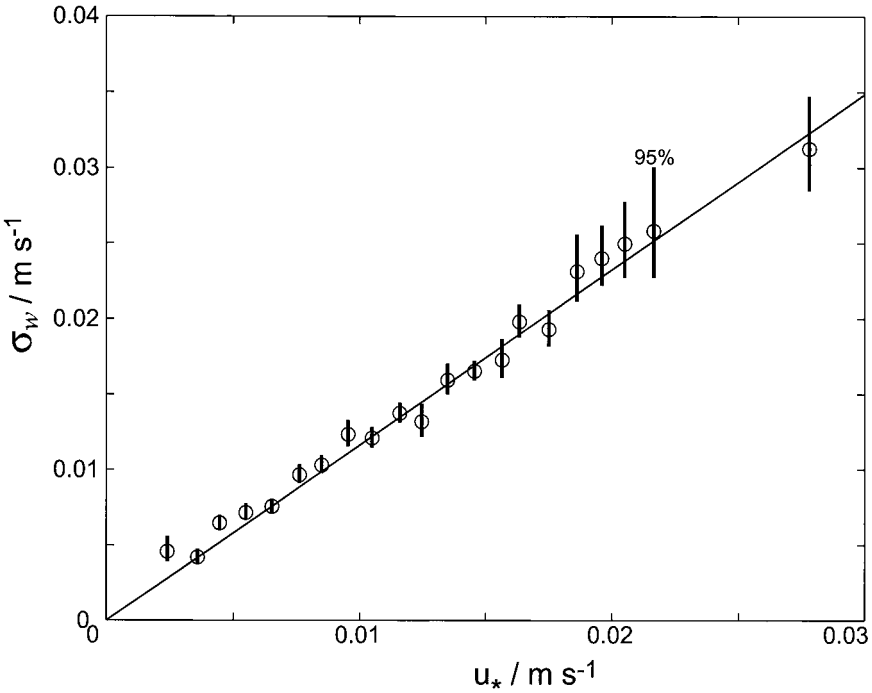

FIG. 4. Root-mean-square vertical velocity σ_w as a function of friction velocity u_*. Line is $\sigma_w = \sqrt{1.35}\, u_*$. Error bars are 95% confidence limits of a χ^2 distribution. [Degrees of freedom are the sum of the degrees of freedom n_i for for each data segment i of duration T, where $n_i = T/(\tau_0 u_*/H)$.]

Sl_{peak} is correlated with u_*, with steeper waves occurring at higher winds. The correlation is stronger for peaks naively chosen from the scalar wave spectra than for the actual windsea peak chosen from the directional wave spectra using the Banner et al. (2000) definition of ''significant spectral peak steepness.''[5] In contrast, the energy at frequencies well above the spectral peak is described accurately by the Phillips (1985) spectrum and varies closely with u_*. Equivalently, the spectral level of the wave slope spectrum at high frequency Φ_{slope} is proportional to u_*. The surface value of the Stokes drift velocity S_0 was computed from both the directional wave spectra and, less accurately, from the scalar wave spectra assuming a unidirectional spectrum. These values are only weakly correlated with u_*. The turbulent Langmuir number $La = \sqrt{u_*/S_0}$ was more likely to be small at low wind speeds, because S_0 is less variable than u_*. Inverse wave ''age'' u_*/C_{peak} is correlated with u_*, with younger waves occurring at higher wind speeds. When any correlation with u_* was removed, neither S_0, La,

[5] Banner et. al. compute the wave height associated with the peak by integrating the spectrum from 0.7 to 1.3 times the peak frequency. They do not specify the directional range of integration; a value of $\pm\pi/8$ around the peak direction is used here.

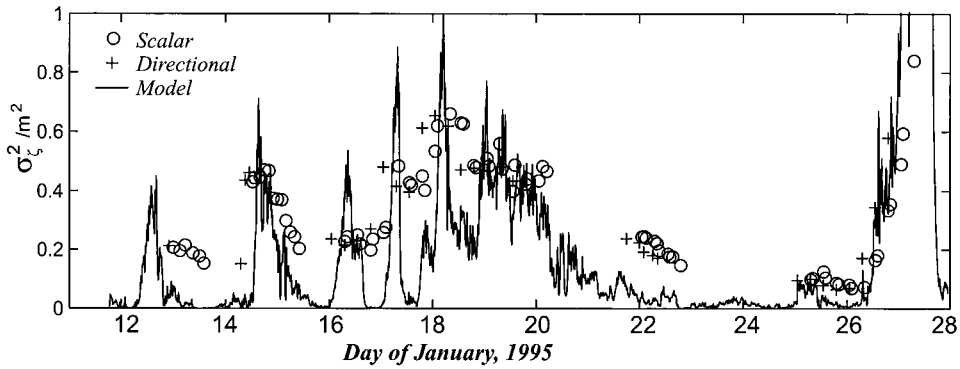

FIG. 5. Mean square surface wave displacement calculated from scalar wave spectra (open circles), from directional wave spectra (pluses) and from a model wave spectrum in equilibrium with the wind forcing.

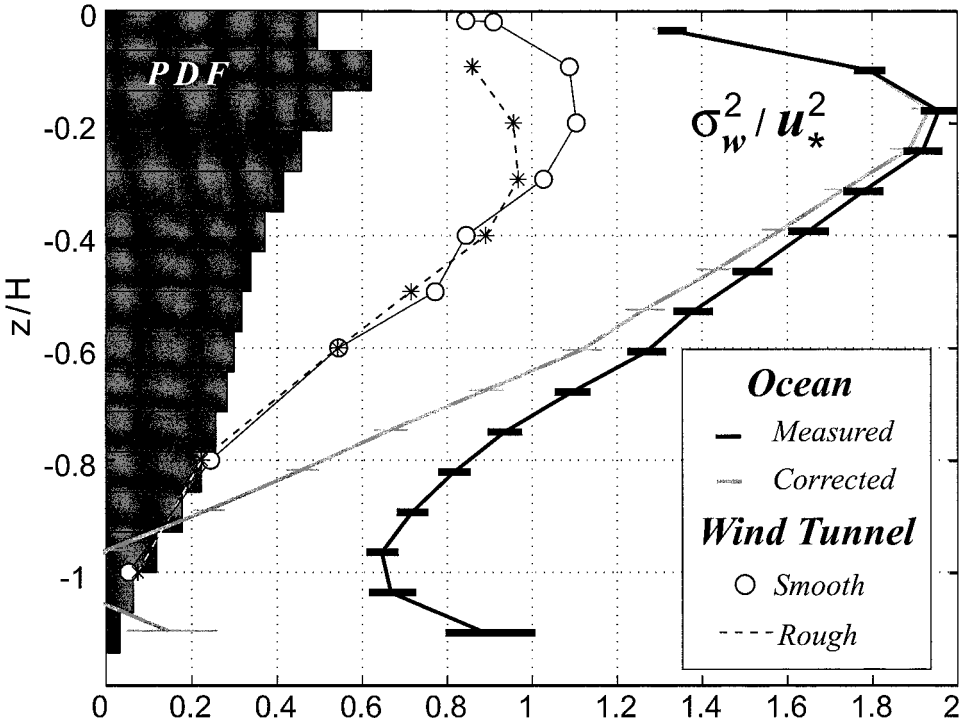

FIG. 6. Scaled vertical kinetic energy $A(z) = \sigma_w^2/u_*^2$ as a function of scaled depth z/H (curve). Error bars are 95% confidence limits of a χ^2 distribution. The degrees of freedom are estimated from the ratio of mean to standard deviation at each depth. The gray profile has been corrected for biases near $Z/H = -1$. Circles represent σ_w^2/u_*^2 for a smooth-wall zero-pressure-gradient turbulent boundary layer; stars represent the same for a rough-wall boundary layer (Hinze 1975). Bars indicate probability distribution of float data on an arbitrary scale.

E_{wave}, C_{peak}, u_*/C_{peak}, Φ_{slope}, nor Sl_{peak} showed any significant relationship with σ_w^2.

Figure 6 shows $A(z)$. Depth is scaled with H in order to minimize the effect of the large variations in H. Float data with $H < 20$ m were excluded in order to avoid large vertical stretching of very thin mixed layers. Float data with $u_* < 0.008$ m s^{-1} were also excluded from the averages because, as indicated in Fig. 4, there is a departure from a linear relationship for low values of u_*. The floats are not uniformly distributed in depth as they should be if they followed water parcels perfectly. The distribution (Fig. 6) is surface intensified, presumably owing to the buoyancy of the floats, and becomes more uniform with increasing wind stress. The floats therefore oversample the more energetic upper part of the mixed layer and bias the value of σ_w^2/u_*^2 upward from 1.27 for a mixed-layer depth average to 1.45 for a time average.

The profile of $A(z)$ does not go to zero at the mixed layer base, as would be expected for mixed layer turbulence. There are several possible reasons. First, water is exchanged between the mixed layer and the underlying stratification in this region. The float data only include particle trajectories that enter and exit the bottom part of the mixed layer from above and do not sample trajectories that start from or remain in the stratification. The measured trajectories are more energetic than the omitted ones, biasing the average energy high. Harcourt et al. (2001) simulates Lagrangian floats in the Labrador Sea and finds (his Fig. 6) the vertical kinetic energy measured by simulated floats to be high by 29% of the peak value.[6] This bias decays upward with a scale of about $0.2H$ in the simulation. Second, internal waves in the stratified interior will cause vertical velocities throughout the mixed layer. The vertical velocity due to hydrostatic internal waves will decay linearly from its value at the mixed layer base to very close to zero at the surface. Nonhydrostatic internal waves will decay faster (D'Asaro 1978), but these have only a small fraction of the total energy. The average σ_w^2 from five floats deployed in the mixed layer base near the start of the measurements was (6 mm s^{-1})^2 or about $0.18u_*^2$. Third, the upward buoyancy of the floats causes them to oversample the more energetic downward-going plumes leaving the surface (D'Asaro et al. 2001) and thus bias the velocity high. Harcourt et al. (2001) models this effect for floats with a bias velocity of 7 mm s^{-1}, which is somewhat larger than is appropriate here. The bias

[6] The peak value of σ_w^2 in the Labrador Sea data is very similar to that in Fig. 6, although the mixed layer depth is about 10 times larger.

extends across the mixed layer with a value of 25% of the peak σ_w^2.

The profile of $A(z)$ was corrected for the first two factors (gray line in Fig. 6). The corrections reduce σ_w^2 at the mixed layer base to slightly below zero, indicating that they alone are more than sufficient to explain the measured nonzero value. The effect of the third factor is probably small. The correct profile of turbulent σ_w^2 probably lies between the gray and black curves and is probably closer to the gray curve than the black curve.

For both measured and corrected profiles $A(z)$ reaches a maximum value between 1.9 and 2 in the upper mixed layer. Turbulent boundary layers driven by shear alone (stars and circles in Fig. 6) show maximum values of σ_w^2/u_*^2 of approximately 1 for both smooth- and rough-walled boundary layers (McPhee and Smith 1976; Hinze 1975). The oceanic profile of turbulent vertical kinetic energy is between 1.75 and 2 times larger than that in these shear-driven boundary layers.

4. Discussion

Surface waves are likely responsible for the enhanced turbulent vertical kinetic energy found here, either through the action of wave breaking or Langmuir circulation. Terray et al. (1996) measured energy dissipation rates near the surface in the ocean boundary layer and found them far above those in wall-bounded boundary layers. They attribute this to surface wave breaking and find the excess energy dissipation equal to the flux of energy F_{ww} from the wind to the waves. Using a large collection of historical surface wave spectra, they find $F_{ww} = \rho u_*^2 \overline{C}$, where $\overline{C}$ is an effective wave phase speed. For a wide range of measured wave spectra, $\overline{C}/C_{\text{peak}}$ is found to be a function of u_*/C_{peak} (see their Fig. 6). When waves are ''old,'' $\overline{C} \approx 10u_*$ and turbulence production due to wave breaking is proportional to u_*^3, as in solid-wall boundary layers, but with a much larger coefficient. The wave spectra measured here indicate that the waves are ''old'' because $u_*/C_{\text{peak}} < 2.2$. Thus Terray et al.'s scaling predicts that the turbulence generated by the waves will scale with u_*, as it does in the absence of waves, but with a much higher turbulence level. A turbulent closure model of this process (Craig and Banner 1994) suggests that the turbulence due to wave breaking should decay rapidly away from the surface and not extend across the entire boundary layer. Physically, this is because the turbulent eddies created by wave breaking are much smaller than the boundary layer thickness. Thus, wave breaking can explain both the high level of turbulence found here and its scaling with u_*, but probably cannot explain why the high level of turbulence is found across the entire boundary layer.

Large-eddy simulation models (Skyllingstad and Denbo 1995; McWilliams et al. 1997) predict vertical kinetic energy profiles for shear-driven, solid-wall boundary layers similar to those shown by the symbols in Fig. 6. When the same models are applied to the ocean, driven by wind stress and surface waves through the CL interaction and using appropriate values of La (D'Asaro and Dairiki 1997), they predict turbulent vertical kinetic energy profiles similar to those shown by the gray line in Fig. 6. The dependence of these results on S_0 has not been explored for these models. Thus, it is unclear whether Langmuir circulation dynamics can explain the observed scaling of σ_w^2 on u_*^2.

The wind stress used here is computed using a drag coefficient C_D so that $\tau_{\text{bulk}} = \rho_{\text{air}} C_D U_{15}^2$, where U_{15} is the wind speed at 15.4 m. The actual stress imparted by the atmosphere on the ocean τ can deviate by up to 50% from τ_{bulk} on the short timescales considered here, owing to time variations in the wind speed and direction and the presence of surface waves that are not aligned with the wind (Rieder and Smith 1998; Dennan et al. 1999). However, these effects are not sufficiently well understood to enable them to be quantified. Large and rapid variations in wind speed are apparent in Fig. 1a; the measured surface wave spectra commonly showed waves propagating from two or more different directions. All of the deviation of σ_w^2 from (1) seen in Fig. 4 could easily be due to deviations of τ from τ_{bulk}.

These observations stand in contrast to those of Smith (1998), who found that the variance in one component of the near-surface horizontal velocity was correlated with S_0^2 rather than with u_*^2 for an approximately 40-h period chosen to have strong Langmuir circulations. Other similar measurements yield conflicting results (Pleuddemann et al. 1996). The properties of the near-surface region may indeed scale differently from the bulk of the mixed layer. The situation may be similar to that for rough- or smooth-wall, shear-driven boundary layers. The flow in the region near the wall depends in detail on the nature of the surface; the flow is quite different for a smooth wall than for a rough wall. However, the net effect of the near-wall region on the bulk of the boundary layer is parameterized by the stress alone.

These results do not necessarily imply that the total turbulent kinetic energy in the ocean boundary layer is higher than in similar shear-driven boundary layers. The simulations of McWilliams et al. (1997) suggest that an effect of the CL interaction is to move kinetic energy from the downwind velocity component to the crosswind and vertical components with little change in the total kinetic energy. Estimates of downwind and crosswind kinetic energies during these measurements will be reported in a future paper.

5. Summary

Vertical velocities in the ocean boundary layer were measured for two weeks at an open ocean, wintertime site using neutrally buoyant floats. Simultaneous measurements of the surface meteorology and surface waves showed a large variability in both wind and wave prop-

erties and only weak correlations between them. Buoyancy forcing was weak.

The mean square vertical velocity in the boundary layer σ_w^2 measured from the vertical motion of the floats was proportional to the squared friction velocity u_*^2 estimated from shipboard meteorological measurements. Thus, $\sigma_w^2 = \overline{A}u_*^2$ with $\overline{A} = 1.35 \pm 0.07$. The deviations from this relation can be attributed entirely to statistical variation and measurement error. The slight buoyancy of the floats causes them to oversample the more energetic upper part of the mixed layer and to bias the measurement of σ_w^2 high near the mixed layer base. Internal wave velocities also contribute nonturbulent vertical velocities. Removing these effects reduces the mixed layer average $\overline{A}$ for turbulent velocities to about 1.0, which is from 1.75 to 2 times that found in solid-wall turbulent boundary layers driven by shear alone.

It is surprising that the measured variations in the boundary layer vertical kinetic energy are not well correlated with the measured variations in surface wave properties. Perhaps this is because the relevant properties of the surface waves are in equilibrium with the wind in these data. The wave measurements, however, show that although the wave breaking rates may be in equilibrium with the wind, their energy, their momentum, and their Stokes drift are not. Other wave properties or other wave measurement systems might yield different results. Similar measurements under short fetch conditions (D'Asaro and Dairiki 1997) produce a higher value of $\overline{A}$ than found here. Perhaps the relationship between waves and boundary layer turbulence is stronger for these younger waves. These issues need to be understood before surface waves can be safely ignored in boundary layer models.

Acknowledgments. This work was supported by NSF Grant OCE-9711650. Cooperation with David Farmer and his group was crucial to the success of the measurements. Special thanks to Geoff Dairiki who played a key role in the development of the Lagrangian floats and in the analysis of their data. Two anonymous reviewers gave valuable insight and advice.

REFERENCES

Banner, M. L., A. V. Babanin, and I. R. Young, 2000: Breaking probability for dominant waves on the sea surface. *J. Phys. Oceanogr.*, **30,** 3145–3160.

Craig, P., and M. L. Banner, 1994: Modeling wave-enhanced turbulence in the ocean surface layer. *J. Phys. Oceanogr.*, **24,** 2546–2559.

D'Asaro, E. A., 1978: Mixed layer velocities induced by internal waves. *J. Geophys. Res.*, **83,** 2437–2438.

——, and G. T. Dairiki, 1997: Turbulence intensity measurements in a wind-driven mixed layer. *J. Phys. Oceanogr.*, **27,** 2009–2022.

——, and R. C. Lien, 2000: Lagrangian measurements of waves and turbulence in stratified flows. *J. Phys. Oceanogr.*, **30,** 641–655.

——, D. M. Farmer, J. T. Osse, and G. T. Dairiki, 1996: A Lagrangian float. *J. Atmos. Oceanic Technol.*, **13,** 1230–1246.

——, K. B. K. B. Winters, and R. Lien, 2001: Lagrangian analysis of a convective mixed layer. *J. Geophys. Res.*, in press.

Dickey, T., D. Manov, R. Weller, and D. Siegel, 1994: Determination of longwave heat flux at the air–sea interface using measurements from buoy platforms. *J. Atmos. Oceanic Technol.*, **11,** 1057–1078.

Drennan, W., H. Graber, and M. A. Donelan, 1999: Evidence for the effects of swell and unsteady winds on marine wind stress. *J. Phys. Oceanogr.*, **29,** 1853–1864.

Fairall, C., E. Bradley, D. Rogers, J. Edson, and G. Young, 1996: Bulk parameterization of air–sea fluxes for tropical ocean global atmosphere coupled ocean atmosphere response experiment. *J. Geophys. Res.*, **101** (C2), 3747–3764.

Harcourt, R. R., E. L. Steffen, R. W. Garwood, and E. A. D'Asaro, 2001: Fully Lagrangian floats in Labrador Sea deep convection: Comparison of numerical and experimental results. *J. Phys. Oceanogr.*, in press.

Hinze, J. O., 1975: *Turbulence.* 2d ed. Mc-Graw Hill, 790 pp.

Leibovich, S., 1983: The form and dynamics of Langmuir circulations. *Annu. Rev. Fluid Mech.*, **15,** 391–427.

Lien, R. C., E. A. D'Asaro, and G. T. Dairiki, 1998: Lagrangian frequency spectra of vertical velocity and vorticity in high–Reynolds number oceanic turbulence. *J. Fluid Mech.*, **362,** 177–198.

McPhee, M., and J. Smith, 1976: Measurements of the turbulent boundary layer under pack ice. *J. Phys. Oceanogr.*, **6,** 696–711.

McWilliams, J., P. Sullivan, and C. Moeng, 1997: Langmuir turbulence in the ocean. *J. Fluid Mech.*, **334,** 1–30.

Melville, W., 1994: Energy dissipation by breaking waves. *J. Phys. Oceanogr.*, **24,** 2041–2049.

Phillips, O. M., 1977: *The Dynamics of the Upper Ocean.* 2d ed. Cambridge University Press, 336 pp.

——, 1985: Spectral and statistical properties of the equilibrium range in wind-generated gravity waves. *J. Fluid Mech.*, **156,** 505–531.

Pierson, W., and L. Moskowitz, 1964: A proposed spectral form for fully developed wind seas based on the similarity theory of S. A. Kitaigorodski. *J. Geophys. Res.*, **69,** 5181–5190.

Pleuddemann, A., J. Smith, D. Farmer, R. Weller, W. Crawford, R. Pinkel, S. Vagle, and A. Gnanadesikan, 1996: Structure and variability of Langmuir circulations during the surface waves processes program. *J. Geophys. Res.*, **101,** 3525–3543.

Rieder, K., and J. A. Smith, 1998: Removing wave effects from the wind stress vector. *J. Geophys. Res.*, **103** (C1), 1363–1374.

Rudnick, D., and R. Ferrari, 1999: Compensation of horizontal temperature and salinity gradients in the ocean mixed layer. *Science,* **283,** 526–529.

Skyllingstad, E., and D. Denbo, 1995: An ocean large-eddy simulation of Langmuir circulations and convection in the surface mixed layer. *J. Geophys. Res.*, **100,** 8501–8522.

Smith, J., 1998: Evolution of Langmuir circulation during a storm. *J. Geophys. Res.*, **103** (C6), 12 649–12 668.

Steffen, E., and E. D'Asaro, 2001: Deep convection in the Labrador sea as observed by Lagrangian floats. *J. Phys. Oceanogr.*, in press.

Stull, R. B., 1988: *An Introduction to Boundary Layer Meteorology.* Kluwer Academic, 666 pp.

Terray, E. A., M. A. Donelan, Y. C. Agrawal, W. M. Drennan, K. K. Kahma, A. J. Williams III, P. A. Hwang, and S. A. Kitaigorodski, 1996: Estimates of kinetic energy dissipation under breaking waves. *J. Phys. Oceanogr.*, **26,** 792–807.

Thais, L., and J. Magnaudet, 1996: Turbulent structure beneath surface gravity waves sheared by the wind. *J. Fluid Mech.*, **328,** 313–344.

Trevorrow, M., 1995: Measurement of ocean wave directional spectra using Doppler side-scan sonar arrays. *J. Atmos. Oceanic Technol.*, **12,** 603–616.